NON-LINEAR FUZZY LOGIC CONTROL FOR MAGNETIC BEARINGS IN LARGE-TIP CLEARANCE- ACTIVE STALL CONTROL APPROACH

SHULIANG LEI, ALAN PALAZZOLO

Texas A&M University, Department of Mechanical Engineering, College Station, TX 77843-3123, USA

ALBERT KASCAK

U. S. Army at NASA Glenn, 21000 Brookpark RD, Cleveland, Ohio 44135, USA

In this paper a prescribed large motion control using active magnetic bearings in a proposed active stall control test rig was developed. A finite element method is employed to model and to synthesize the flexible shaft in a closed loop system. A linearized model of the stall rig using conventional PD controllers to 16 magnetic poles (4 opposing C-cores) yields stability and frequency responses. In the mean time the nonlinear model is studied to consider the Ampere's Law, Faraday's Law and the Maxwell stress tensor. A fuzzy logic control system is then designed to show the advantages over the conventional controllers with the fully nonlinear model.

1. INTRODUCTION

The development of magnetic bearings in rotating machinery has increased significantly due to its low power loss with high-speed operations. Since the shaft and the bearing assembly have no contact between one another, frictional loss, which grows drastically with speed increase, is nearly eliminated. Active magnetic bearings require closed loop feedback, which offers a way to support the rotating shaft as well as to control the vibration. In most industrial applications, the feedback system includes a linear PID controller with compensators, power amplifiers, magnetic actuators and inductive eddy current or optical sensors [1]. In addition to the widely applied PID controllers, advanced control strategies such as optimal control [2], μ-synthesis control [5], H-∞ control [6,8] can be found in some applications. All these methods are based on linear systems theory and need linear models. Nonlinear control techniques were also applied to active magnetic bearings. Sliding mode control and fuzzy logic based control can be found in several papers.

In the applications of aircraft engines, in order to suppress rotating stall in a high-speed compressor wheel, it is desired to shake the wheel at a large amplitudes while maintaining the rotor system stable. Electromagnetic shakers and magnetic bearings have been used for actuators in vibration control. In the case of magnetic shaker with the nonlinear models, there are some difficulties to obtain large whirl orbits because of system instability. By carefully designing a PD controller the shaking orbit radius can be increased but only to a limited value in the stable region.

Motivated by the capability of dealing with nonlinearities of the problem, fuzzy logic has been introduced for control of magnetic bearing system. Although sliding mode control can yield robust performance against modeling error, it is difficult to achieve fast switching required. Fuzzy logic theory was first established in Zadeh's seminal paper [9] in 1965. Since then it has been considered as an effective means in various control problems. An idea of applying fuzzy logic to dynamics systems was introduced in early 70's by Mamdani [10]. The Mamdani architecture of fuzzy logic controller is build up based on qualitative and empirical knowledge of human beings. Later Takagi and Sugeno established a fuzzy model [11], called Takagi-Sugeno model, which can be more easily used for analytical purpose.

The AMB nonlinear model considers the three cases: nonlinear B-H curve, Ampere's Law and Maxwell stress tensor. Fuzzy logic control is constructed by designing a rule base to implement a non-linear control strategy. The antecedent and consequent of each rule operate on the positions of input and output variables in predefined membership functions. These membership functions possess qualitative descriptions which generalize the notion of assigning a single degree to a specific response severity or corrective action level. Researchers in the area of AMB using fuzzy logic control are mainly based on

simple model such as lumped mass model or rigid body model [12] [13]. Some application needs to recursively tune the rules to achieve better performances [14]. While these results are absorbing, they can not deal with a flexible shaft with a dimension of over hundreds of structural states plus control variables. The stall-rig model consists of a rotating shaft with a compressor wheel. Finite element method is used to describe the flexible rotor in designing a suitable control and analyzing the system behavior. The front bearing is an active magnetic bearing system, which includes feedback between non-collocated sensors and actuators, via controllers. The shaft is divided into 23 elements and at node 17, an oil film bearing is employed to support the rotor system. The magnetic bearing is located at node 9. The non-collocated sensors are placed at node 7 and have outputs directed PD controllers. The control signals are then directed to power amplifiers to produce control currents, which drive the coils of the magnetic bearings to control the rotor system. The shaking voltages are applied to a summing point at the control output to force the shaft to execute motions that alter the compressor wheel's tip clearance and inhibit stall cell formation.

Fuzzy logic controllers for active magnetic bearings are synthesized and designed for suppression of imbalance vibration and to increase the shaking orbit radius. The main objective of this paper is to develop robust controllers for maintaining magnetic bearing system stability against imbalance and external shaking forces or voltages for linear and nonlinear models. Applying the basic magnetic bearing theory yields a fully nonlinear model. Based on the nonlinear magnetic bearing model, linearization is carried out to formulate a complete linear model for analysis. The PD controller and the fuzzy logic controllers based on Mamdani architecture are synthesized and designed. The superiority of nonlinear fuzzy logic control over linear PD control is also shown. Simulation results for each type of controllers are provided and their performance specifications can be compared accordingly.

2. SYSTEM MODEL

2.1. MAGNETIC BEARING FORCE

Consider the 2 opposing magnetic C-cores shown in figure 1:

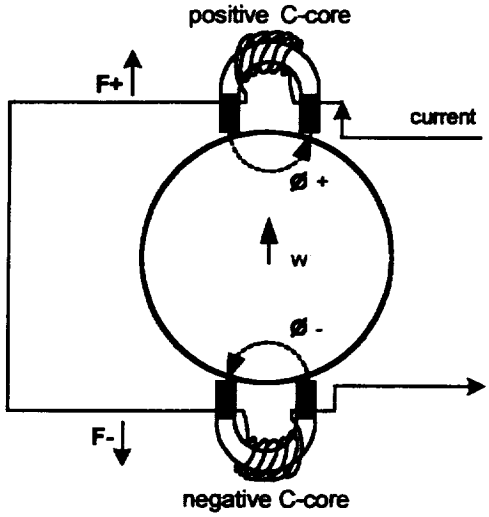

Figure 1. Schematic of 2 opposing C-cores

According to Ampere's law, the magnetic flux density ϕ^+ in the positive C-core is

$$\phi^+ = \frac{(N_B i_B + N_c i)}{2w^+}\mu_0 A_a = \frac{(N_B i_B + N_c i)}{2(g_0 - w)}\mu_0 A_a \tag{1}$$

The magnetic flux density ϕ^- in the negative C-core is

$$\phi^- = \frac{(N_B i_B - N_c i)}{2w^-}\mu_0 A_a = \frac{(N_B i_B - N_c i)}{2(g_0 + w)}\mu_0 A_a \tag{2}$$

where g_0 is the air gap of the magnetic bearing and w is the displacement of the rotor in positive direction. The corresponding flux density in the positive magnetic path and the negative magnetic path can then be written as:

$$B^+ = \frac{\phi^+}{A_a} = \frac{(N_B i_B + N_c i)}{2(g_0 - w)}\mu_0, \quad B^- = \frac{\phi^-}{A_a} = \frac{(N_B i_B - N_c i)}{2(g_0 + w)}\mu_0 \tag{3}$$

Note that Ampere's Law yields flux expressions that are nonlinear functions of the shaft displacement w.

A second nonlinearity occurs when the Maxwell stress tensor formula is applied to obtain the resultant electromagnetic force of the two opposing C-cores:

$$F = [(B^+)^2 \frac{A_a}{\mu_0} - (B^-)^2 \frac{A_a}{\mu_0}] \cos\delta \tag{4}$$

where

$$(B^-)^2 = \frac{(N_B i_B - N_c i)^2}{4(g_0 + w)^2} \mu_0{}^2, \qquad (B^-)^2 = \frac{(N_B i_B - N_c i)^2}{4(g_0 + w)^2} \mu_0{}^2 \tag{5}$$

This yields:

$$F = \eta^2 \cos\delta \frac{A_a \mu_0}{4} [(\frac{N_B i_B + N_c i}{g_0 - w})^2 - (\frac{N_B i_B - N_c i}{g_0 + w})^2] \tag{6}$$

The related parameters for the example considered are :

$\mu_0 = 4\pi \times 10^{-7}$

$A_a = \frac{6}{39.37^2} (m^2)$, *area per pole*

$g_0 = \frac{0.02}{39.37} (m)$, *air gap*

$\delta = 360^\circ / (16 \times 2) = 11.25^\circ$, *half angle between poles*

$\eta = 0.9$ *derate factor*

$i_B = 30(A)$, *bias current*

$N_B = 40$ (*turns per C – core*), *bias coil*

$N_c = 16$ (*turns per C – core*), *control coil*

2.2. COIL INDUCTANCE AND VOLTAGE

According to Faraday' s law, the coil voltage in each C-core can be written as follws: positive C-core

$$V_L^+ = N_c \frac{d\phi^+}{dt} = \frac{N_c^2 \mu_0 A_a}{2} \frac{d}{dt} (\frac{i}{w^+}) \tag{7}$$

negative C-core

$$V_L^- = N_c \frac{d\phi^-}{dt} = \frac{N_c^2 \mu_0 A_a}{2} \frac{d}{dt} (\frac{i}{w^-}) \tag{8}$$

or:

$$V_L^+ = \frac{N_c^2 \mu_0 A_a}{2w^+}\frac{di}{dt} + \frac{N_c^2 \mu_0 A_a}{2} i \frac{d}{dt}\left(\frac{1}{w^+}\right)$$
$$= L^+ \frac{di}{dt} + \frac{N_c^2 \mu_0 A_a}{2} i \frac{d}{dt}\left(\frac{1}{g_0 + w}\right) \tag{9}$$

and

$$V_L^- = \frac{N_c^2 \mu_0 A_a}{2w^-}\frac{di}{dt} + \frac{N_c^2 \mu_0 A_a}{2} i \frac{d}{dt}\left(\frac{1}{w^-}\right)$$
$$= L^- \frac{di}{dt} + \frac{N_c^2 \mu_0 A_a}{2} i \frac{d}{dt}\left(\frac{1}{g_0 + w}\right) \tag{10}$$

where

$$L^+ = \frac{N_c^2 \mu_0 A_a}{2}\left(\frac{1}{g_0 - w}\right), \qquad L^+ = \frac{N_c^2 \mu_0 A_a}{2}\left(\frac{1}{g_0 + w}\right) \tag{11}$$

are the non-linear inductances of the coils on the two opposing C-cores.

Considering the coil resistance R, the voltage drop across the power amplifier output terminals for two opposing C-cores becomes:

$$V = 2Ri + L^+ \frac{di}{dt} + \frac{N_c^2 \mu_0 A_a}{2} i \frac{d}{dt}\left(\frac{1}{g_0 - w}\right) + L^- \frac{di}{dt} + \frac{N_c^2 \mu_0 A_a}{2} i \frac{d}{dt}\left(\frac{1}{g_0 + w}\right) \tag{12}$$

Eqs. 10-12 show the nonlinearity that is contained in the voltage expression obtained from Faraday's Law.

2.3. FLUX DENSITY SATURATION

Due to the non-linear property of the ferromagnetic materials, the flux density in the magnetic circuit will saturate with increase of exciting coil current. The AMB forces saturate accordingly due to the saturation of the magnetic field.

For simplicity , suppose the maximum flux density is 2 Teslas:

$$B^{+}_{\max} = B^{-}_{\max} = 2 \ (Teslas) \tag{13}$$

Then we have for the maximum AMB forces expressed as:

$$F^{-}_{\max} = F^{+}_{\max} = \eta^2 \cos\delta (B^{+}_{\max})^2 \frac{A_a}{\mu_0} = 4\eta^2 \cos\delta A_a \mu_0 \tag{14}$$

The saturation of flux density B limits the maximum force :

$$F_{\max} = (B^{+}_{\max})^2 \frac{A_a}{\mu_0} \tag{15}$$

The above result is valid for each opposing C-core pair (2 opposing C-cores).

2.4. CLOSED LOOP SYSTEM

The basic configuration of one control channel is shown in Figure 2.:

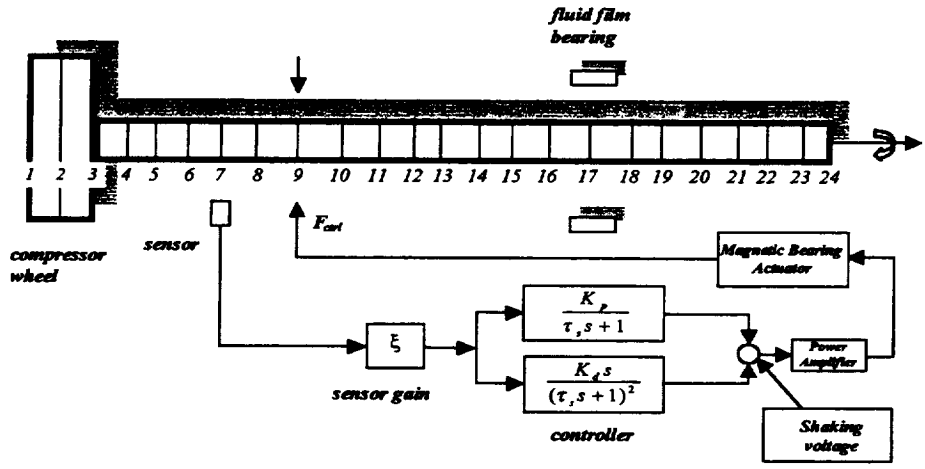

Figure 2. Finite element model of shaft plus feedback control path

In this diagram, we use PD controllers in the feedback loop. A more elegant nonlinear fuzzy logic controller will be described later. It can be seen from this configuration that the shaft is divided into 23 elements. Dimensional data for this model are given in the Appendix. The sensor is located at node 7 and the actuator is located at node 9: this is a non-collocated system. An oil film bearing is placed at node 17 to support the other end of the shaft (see Appendix). The sensor measures the displacement signal of the rotor and feeds the signal to the controller. The controller synthesizes the input signal to generate output voltage to the power amplifier (P.A.), which in turn produces the control current for the magnetic bearing coil to support the rotor. The compressor wheel is located in the first two elements and the operating rotor spinning rate is set to $\Omega=17000\ rpm$

3. LINEAR ANALYSIS

3.1. LINEARIZATION

The magnetic bearing used to support and shake the rotor has 16 poles, which constitutes 4 C-core -pairs. The 4 magnetic bearing system consists of 8 C-cores distributed around the circle at uniform angles of 45 degrees. Each C-core has 2 poles, N and S, two opposing C-cores have 4 poles. Totally the system has 16 poles evenly distributed at an angle of 22.5 degrees. Figure 3 shows the configuration of the 4 C-core-pairs.

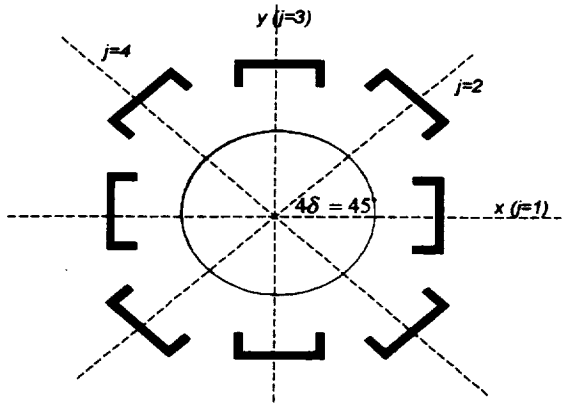

Figure 3. Configuration of the 4 C-core-pairs

Rewrite F for the j-th *(j=1,2,3,4)* C-core pole pair as

$$F = \eta^2 \cos\delta \frac{A_a \mu_0}{4}[(\frac{N_B i_B + N_c i}{g_0 - w})^2 - (\frac{N_B i_B - N_c i}{g_0 + w})^2]$$
$$= k_\alpha[(\frac{N_B i_B + N_c i}{g_0 - w})^2 - (\frac{N_B i_B - N_c i}{g_0 + w})^2] \quad (16)$$

where

$$k_\alpha = \eta^2 \cos\delta \frac{A_a \mu_0}{4} \quad (17)$$

Linearize the force at *i=0* and *w=0:*

$$\frac{dF}{di} = 2k_\alpha[\frac{(N_B i_B + N_c i)N_c}{(g_0 - w)^2} + \frac{(N_B i_B - N_c i)N_c}{(g_0 + w)^2}] \Big|_{\substack{i=0 \\ w=0}} = 4k_\alpha \frac{i_B^2}{g_0^2} N_B N_c \quad (18)$$

$$\frac{dF}{dw} = 2k_\alpha[\frac{(N_B i_B + N_c i)^2}{(g_0 - w)^3} + \frac{(N_B i_B - N_c i)^2}{(g_0 + w)^3}] \Big|_{\substack{i=0 \\ w=0}} = 4k_\alpha N_B^2 \frac{i_B^2}{g_0^3} \quad (19)$$

Therefore,

$$\mathbf{F} = [F_x(x, y, i_x, i_y),\ F_y(x, y, i_x, i_y)]$$
$$= \begin{bmatrix} \frac{\partial F_x}{\partial g_1} & \frac{\partial F_x}{\partial g_2} & \frac{\partial F_x}{\partial g_3} & \frac{\partial F_x}{\partial g_4} \\ \frac{\partial F_y}{\partial g_1} & \frac{\partial F_y}{\partial g_2} & \frac{\partial F_y}{\partial g_3} & \frac{\partial F_y}{\partial g_{41}} \end{bmatrix} \begin{bmatrix} \frac{\partial g_1}{\partial x} & \frac{\partial g_1}{\partial y} \\ \frac{\partial g_2}{\partial x} & \frac{\partial g_2}{\partial y} \\ \frac{\partial g_3}{\partial x} & \frac{\partial g_3}{\partial y} \\ \frac{\partial g_4}{\partial x} & \frac{\partial g_4}{\partial y} \end{bmatrix} \begin{bmatrix} x \\ y \end{bmatrix} + \begin{bmatrix} \frac{\partial F_x}{\partial i_x} & \frac{\partial F_x}{\partial i_y} \\ \frac{\partial F_y}{\partial i_x} & \frac{\partial F_y}{\partial i_y} \end{bmatrix} \begin{bmatrix} i_x \\ i_y \end{bmatrix} \quad (20)$$

Geometric consideration of the 4 C-core pairs gives the following relations:

$$g_1 = x$$
$$g_2 = x\cos(\pi/4) + y\sin(\pi/4)$$
$$g_3 = y \quad (21)$$
$$g_4 = x\cos(3\pi/4) = y\sin(3\pi/4)$$

Then,

$$\mathbf{F} = [F_x(x, y, i_x, i_y),\ F_y(x, y, i_x, i_y)]$$
$$= \begin{bmatrix} \frac{\partial F_x}{\partial g_1} & \frac{\partial F_x}{\partial g_2} & \frac{\partial F_x}{\partial g_3} & \frac{\partial F_x}{\partial g_4} \\ \frac{\partial F_y}{\partial g_1} & \frac{\partial F_y}{\partial g_2} & \frac{\partial F_y}{\partial g_3} & \frac{\partial F_y}{\partial g_4} \end{bmatrix} \begin{bmatrix} 1 & 0 \\ \sqrt{2}/2 & \sqrt{2}/2 \\ 0 & 1 \\ -\sqrt{2}/2 & \sqrt{2}/2 \end{bmatrix} \begin{bmatrix} x \\ y \end{bmatrix} + \begin{bmatrix} \frac{\partial F_x}{\partial i_x} & \frac{\partial F_x}{\partial i_y} \\ \frac{\partial F_y}{\partial i_x} & \frac{\partial F_y}{\partial i_y} \end{bmatrix} \begin{bmatrix} i_x \\ i_y \end{bmatrix} \tag{22}$$

After algebraic manipulations:

$$\mathbf{F} = K_{pos} \begin{bmatrix} 1 & 0 \\ 0 & 1 \end{bmatrix} \begin{bmatrix} x \\ y \end{bmatrix} + \begin{bmatrix} \frac{\partial F_x}{\partial i_x} & \frac{\partial F_x}{\partial i_y} \\ \frac{\partial F_y}{\partial i_x} & \frac{\partial F_y}{\partial i_y} \end{bmatrix} \begin{bmatrix} i_x \\ i_y \end{bmatrix} \tag{23}$$

where $K_{pos} = 8k_\alpha \frac{i_B^2}{g_0^3} N_B$ is the position stiffness.

For the current stiffness, note that

$$\begin{aligned} i_1 &= i_x \\ i_2 &= i_x \cos(\pi/4) + i_y \sin(\pi/4) \\ i_3 &= i_y \\ i_4 &= i_x \cos(3\pi/4) + i_y \sin(3\pi/4) \end{aligned} \tag{24}$$

Therefore:

$$\begin{bmatrix} \frac{\partial F_x}{\partial i_x} & \frac{\partial F_x}{\partial i_y} \\ \frac{\partial F_y}{\partial i_x} & \frac{\partial F_y}{\partial i_y} \end{bmatrix} = N_B N_c 8k_\alpha \frac{i_B}{g_0^2} \begin{bmatrix} 1 & 0 \\ 0 & 1 \end{bmatrix} \tag{25}$$

where $K_i = N_B N_c 4k_\alpha \frac{i_B}{g_0^2}$ is the current stiffness.

The total linearized resultant force is:

$$\mathbf{F} = K_{pos} \begin{bmatrix} 1 & 0 \\ 0 & 1 \end{bmatrix} \begin{bmatrix} x \\ y \end{bmatrix} + K_i \begin{bmatrix} 1 & 0 \\ 0 & 1 \end{bmatrix} \begin{bmatrix} i_x \\ i_y \end{bmatrix} \tag{26}$$

To obtain the linear electric load, we ignore the coil inductance difference in the two opposing C-cores due to the radial displacement of the rotor, that is, let

$$w^+ = w^- = g_0$$

Then $L^+ = L^- = L$, where

$$L = \frac{N_c^{\,2} \mu_0 A_a}{2 g_0} \tag{27}$$

For two opposing C-cores, the linear electric load is

$$V = 2Ri + 2L \frac{di}{dt} \tag{28}$$

3.2. STABILITY AND STEADY STATE ANALYSIS

The linearized closed loop equation is expressed as:

$$\dot{\mathbf{Z}} = \mathbf{A}\,\mathbf{Z} + \mathbf{B}\mathbf{u} \tag{29}$$

where

$\mathbf{Z} = [x_1\ y_1\ \theta_{x1}\ \theta_{y1}\ x_2\ y_2\ \theta_{x2}\ \theta_{y2}\ .....x_N\ y_N\ \theta_{yN}\ \theta_{zN}]^T$ is the state variable vector of the closed loop system,

Bu represents external disturbances, i.e. imbalance and shaking input

A = closed loop system matrix where the feedback control forces are included.

The system stability property is determined by the eigenvalues of the closed loop system matrix A. If all the real parts of the eigenvalues of A are negative, i.e. the complex eigenvalues are all located on the left half plane, the system is stable. For a stable system, the steady state solution is given as follows:

$U = \hat{U} e^{j\omega t}$ where ω = shaking frequency

This lead to

$$\begin{aligned} & \hat{U}j\omega e^{j\omega t} = A\hat{U}e^{j\omega t} + \hat{F}e^{j\omega t} \\ \Rightarrow \quad & j\omega\hat{U} = A\hat{U} + \hat{F} \\ \Rightarrow \quad & (j\omega - A)\hat{U} = \hat{F} \\ \Rightarrow \quad & \hat{U} = (j\omega - A)^{-1}\hat{F} \end{aligned}$$

Figure 4 show the amplitude of the compressor wheel (node 2 and node9) with respect to the shaking frequency.

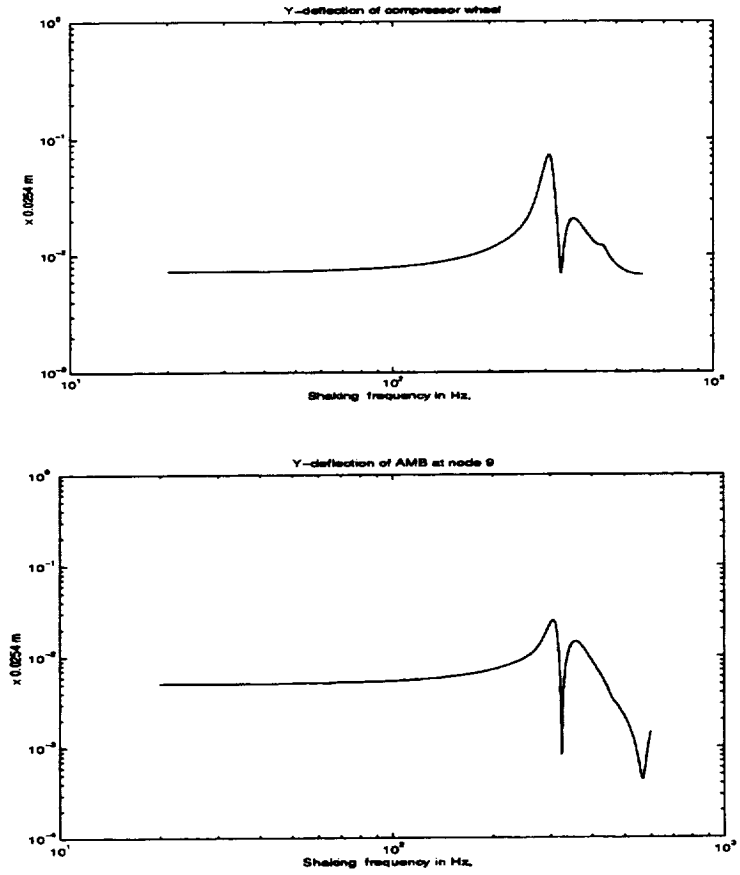

Figure 4. Compressor wheel amplitude vs. shaking frequency

The frequency responses are obtained with the following conditions:

Shaking frequency varies from 20 Hz to 600 Hz, shaking voltage=66 v

Rotor spinning rate Ω=17000 rpm

The following table shows the steady state displacements in the x and y directions at node 2, node 5, node 9 and node 17, when the shaking frequency =200 Hz, respectively:

Node number	*2*	*5*	*9*	*17*
Displacement *(mm)*	*0.292*	*0.241*	*0.178*	*0.0355*

Note that this is a linear response prediction and the nonlinear response amplitudes were less than 0.254mm.

4. TRANSIENT RESPONSE SIMULATION WITH PD CONTROLLERS

The simulation was carried out with the following parameters:

PD controllers:

Proportional control path: $\frac{K_p}{\tau_s s+1}$, Derivative control path: $\frac{K_d s}{(\tau_s s+1)^2}$

where $Kp = 65$, $Kd = 0.008$, $\tau_s = \frac{1}{2\pi \times 5000}$

Power amplifier DC gain = 1

Sensor gain : $\xi = 200$

Rotor spin rate: $\Omega = 17000$ rpm

Shaking voltage frequency: *200Hz*

SIMULATION WITH LINEAR MODEL:

Results for the linear model are shown in Table 1

Table 1. Linearized model forced response results

V(shaking)	Radius of orbit At node 2 (*mm*)	Power amplifier voltage (*v*)	Power amplifier current (*A*)
20	*0.0889*	*50*	*16*
45	*0.2032*	*110*	*35*
80	*0.3556*	*180*	*62*

It can be seen that the radius of the orbit at node 2 is proportional to the magnitude of the shaking voltage. The magnitude of the shaking voltage increases linearly with time until it reaches the desired steady state value. Figure 5 shows a linear system shaking orbit and power amplifier voltage for *Vshaking=80 v*:

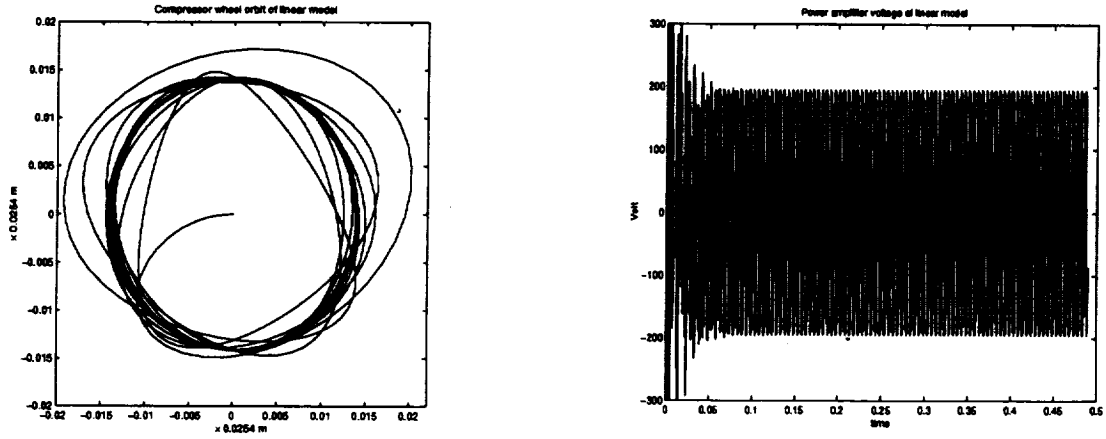

Figure 5. Linear model vibration response at node 2

SIMULATION WITH NON-LINEAR MODEL:

In the non-linear model, we include the nonlinear magnetic bearing forces, the nonlinear electric load expression and the saturation of the flux density. The following table summarizes the simulation result:

V(shaking) (v)	Radius of orbit At node 2 (mm)	Power amplifier voltage (v)	Power amplifier current (A)
20	*0.0635*	*17*	*5*
30	*0.0965*	*25*	*8*
45	*0.1524*	*40*	*12*
46	*0.1549*	*46*	*14*
50	*diverge*		

Figure 6 shows a shaking orbit and power amplifier voltage for the fully non-linear model when $Vshaking=46v$. Not ethat the target of $0.25mm$ could not be achieved with a PD control. This was true even over an exhaustive range of K_p and K_d values.

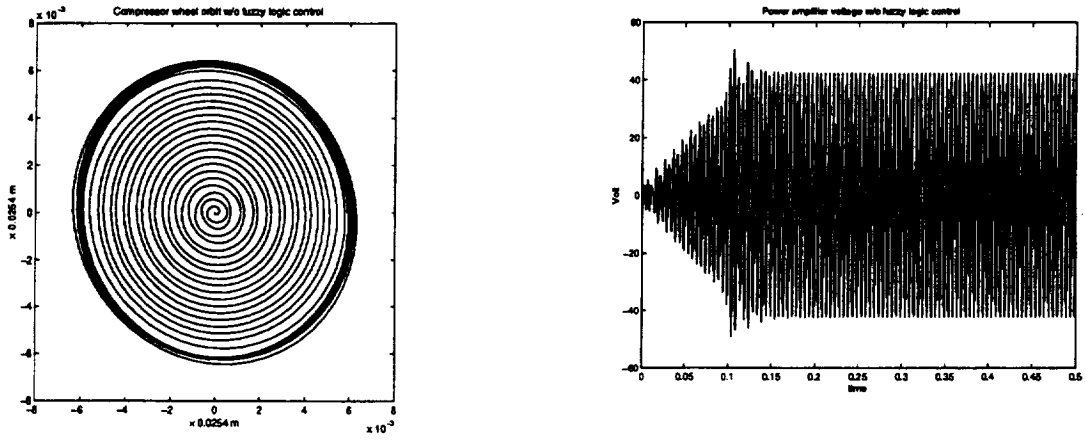

Figure 6. Nonlinear model vibration response of node 2

5. FUZZY LOGIC CONTROL

From the simulation results, it can be seen that with the linear model, the radius of the shaking orbit can be easily made greater than *0.25mm*. For the nonlinear model, the maximum radius is *0.16mm* at a shaking voltage of *46v*. Further increase of the shaking voltage leads to system divergence.

For the active stall control studies, it is desired to obtain a shaking radius of *0.25mm* to reduce the stall of the compressor wheel. This target can not be attained with the PD controller. A fuzzy logic controller is introduced in the control loop to overcome this difficulty. The *0.25mm* shaking radius can be reached by adding fuzzy logic controllers with Mamdani architecture.

Fuzzy logic is an intuitive way to map an input space to an output space. In our case, the input space is position voltage v_p and the rate of change voltage v_d, and the output space is the control voltage v_c. To employ a fuzzy logic controller, we define input and output membership functions which describe the truth of any statement as a matter of degree. More precisely, a membership function is a curve that defines how each point in the input space is mapped to a membership value between 0 and 1. Then based on experts' heuristic knowledge about how to control a system, a rule base is formulated holding the knowledge of how to best control the system.

The fuzzy logic controller is formed as follows:

The 2 inputs called v_p and v_d, and one output denoted as v_c. Triangular and trapezoidal shapes are used to define the membership functions.

The 3 input membership functions for v_p are: *neg, zero, pos*

The 3 input membership functions for v_d are: *neg, zero, pos*

The 5 output membership functions for v_c are: *vneg, neg, zero, pos, vpos*

The following figures depict the input and output membership functions:

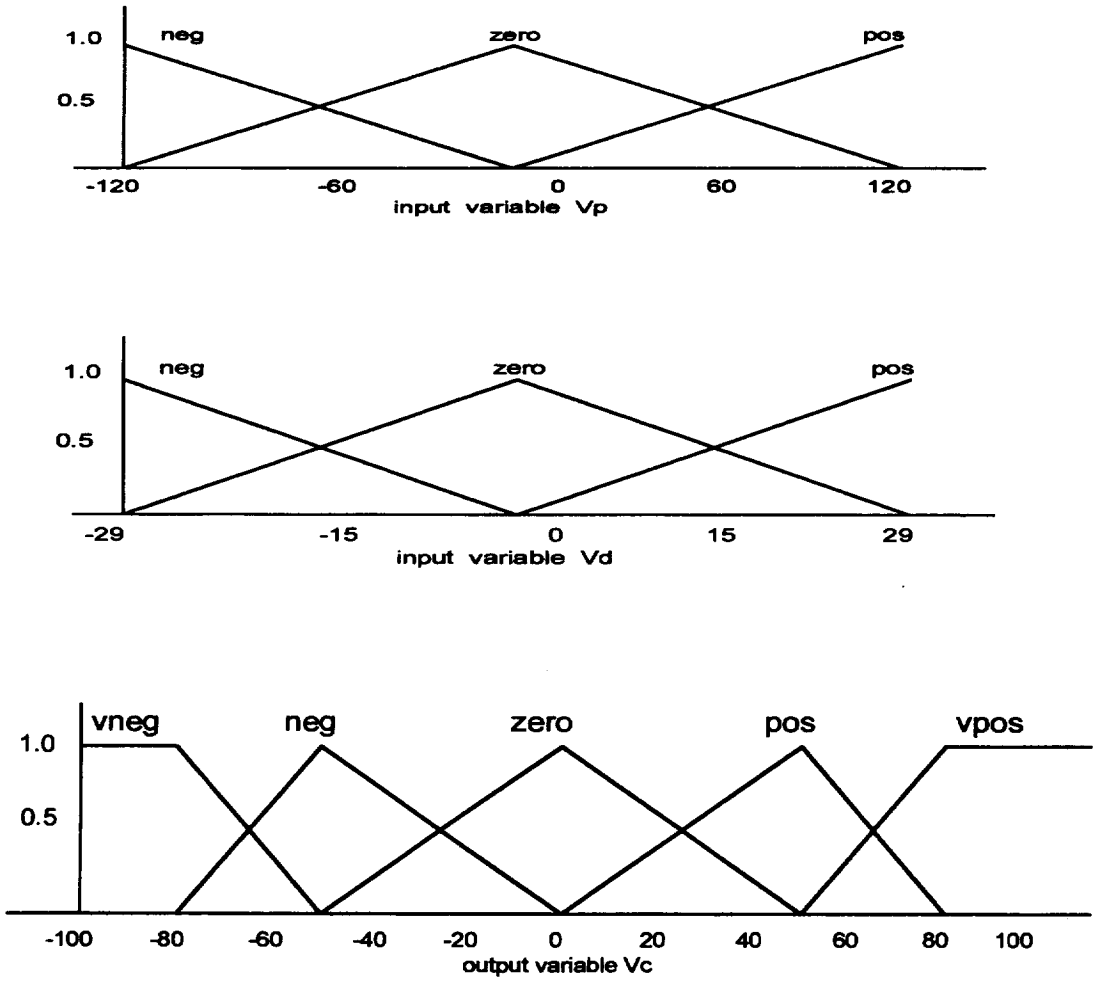

Figure 7. Input and output membership functions

The rule base can be described in the following compact form:

Inputs	v_p: *neg*	v_p:*zero*	v_p: *pos*
v_d: *neg*	*vneg*	*neg*	*zero*
v_d: *zero*	*neg*	*zero*	*pos*
v_d: *pos*	*zero*	*pos*	*vpos*

The above table formulates 9 rules. For example, the first rule is:

if v_p is neg and v_d is neg , then v_c is vneg.

Schematically, the closed loop system with fuzzy logic controller is depicted in Figure 8:

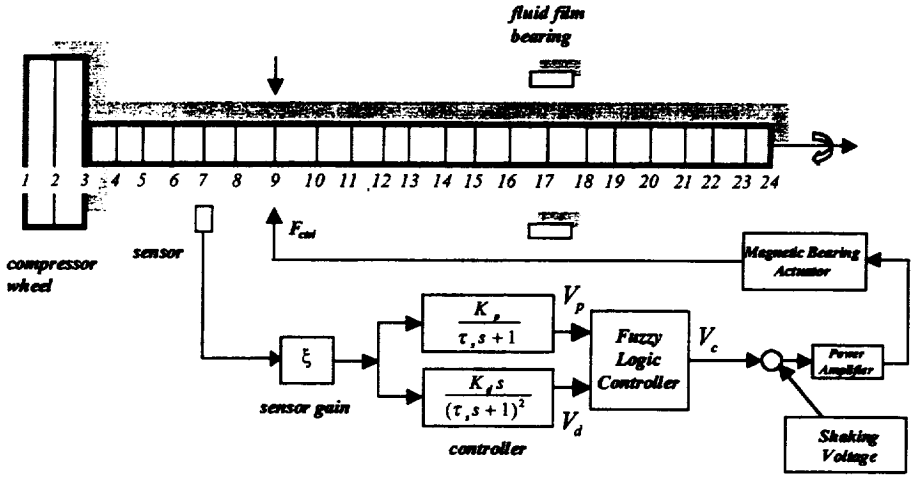

Figure 8. PD controllers with fuzzy logic control stage

The results with the fuzzy logic controller are

V_{shaking} (v)	*Radius of orbit*	*Power amplifier volt. (v)*	*Power amplifier current(A)*
45	*0.25 mm*	*220*	*70*

It can be seen that the cost paid for the larger shaking radius is higher power amplifier voltage and current. However, these are within the allowable limits for the selected power amplifier. Figure 9 shows the wheel orbit and the power amplifier voltage with the fuzzy logic control stage.

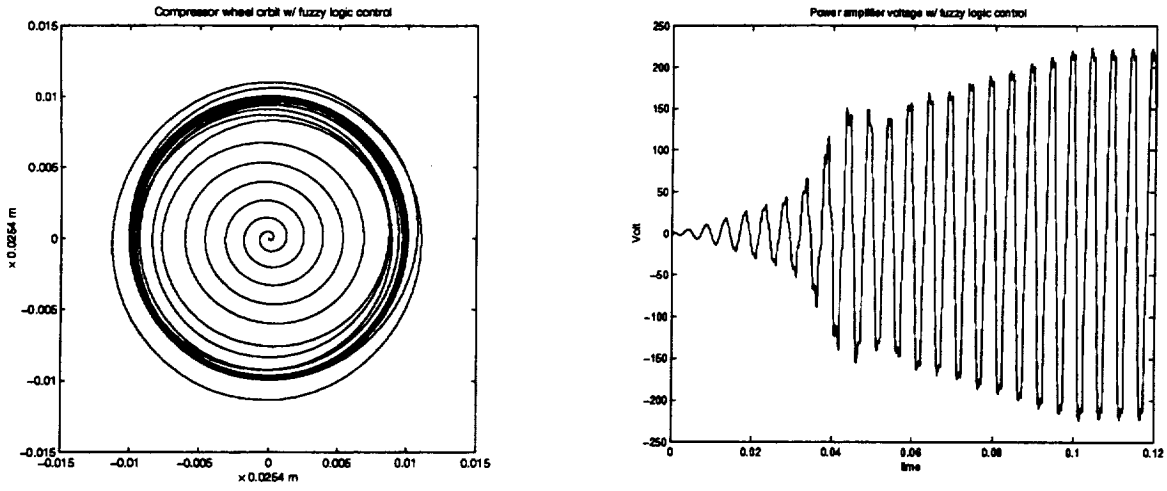

Figure 9. Shaking voltage response with fuzzy logic control stage

6. CONCLUSION

In the closed loop analysis, frequency response with the shaking voltage of *66 v* is given for the magnetic front bearing system. When the shaking frequency is *200 Hz*, the shaking radius of node 2 reaches *0.29 mm* with the designed PD control.

We have also shown that in the transient simulation, the linear model can reach higher shaking orbit radius. When the shaking voltage is as high as 80 volts, the simulation still converges and the orbit radius at node 2 is greater than *0.25 mm*. However the linearized force assumptions are shown to be invalid by comparing the results between the linear and nonlinear models.

For the full nonlinear case it is impossible to reach *0.25mm* radius with conventional PD controllers. Further increase of the shaking voltage will result in simulation divergence. However, the large shaking amplitudes required for the NASA stall-rig necessitates a fully nonlinear model. Although a linear approach can be used as a preliminary means to analyze the system, it is not appropriate for obtaining accurate results. By employing a fuzzy expert system, it has been shown that the shaking orbit

radius may be increased 50% greater than that with the conventional PD controllers. The fuzzy rule base system used in this approach is very simple and direct, so it is easy to implement on a real time basis.

REFERENCES

[1] C. Kim, A. B. Palazzolo *et al* 1995 *Transactions of the ASME* 117, 162-170. Eddy current effects on the design of rotor-magnetic bearing systems.

[2] Ho-seop Jeong *et al* 1994 *Proceed. International Symposium on Mag. Bearings* 4, 23-28. Modeling and control of cone-shaped active magnetic bearing system.

[3] F. Matsumura *et al* 1986 *IEEE Transactions Magnetics* MAG-22 3, 196-203. System modeling and control design of a horizontal shaft magnetic bearing system.

[4] Y. Zhuravlyov 1998 *Proceed. International Symposium on Mag. Bearings* 6, 587-596. Linear quadratic optimal control of active magnetic bearings for high speed rotor.

[5] K. Nonami *et al* 1994 *Proceed. International Symposium on Mag. Bearings* 4, 73-78. μ-Synthesis flexible rotor magnetic bearing control.

[6] F. Carrere *et al* 1994 *Proceed. International Symposium on Mag. Bearings* 4, 65-72. H∞ control design of flexible rotor magnetic bearings.

[7] M. Fujita *et al* 1993 *IEEE Control System Magazine*13-4, 57-65. Loop shaping based robust control of a magnetic bearing.

[8] F. Matsumura *et al* 1996 *IEEE Trans. Control System Tech.* 4-5, 484-493. Application of gain scheduled H∞ robust controllers to a magnetic bearing.

[9] L. Zadeh 1965 *Information and Control* 8-3, 338-353. Fuzzy sets.

[10] E. Mamdani 1976 *Int. J. Man-Machine Stud.* 6, 669-678. Advances in the linguistic synthesis of fuzzy controllers.

[11] K. Tagaki and M. Sugeno 1985 *IEEE Trans. Syst., Man, Cybern.* 15, 116-132. Fuzzy identification of systems and its application to modeling and control.

[12] H. Koskinen *et al* 1994 *Proceed. International Symposium on Mag. Bearings* 4, 89-93. Fuzzy logic in active magnetic bearing control.

[13] B. Weidemann *et al* 1994 *Proceed. International Symposium on Mag. Bearings* 4, 59-64. A nonlinear fuzzy control for magnetic bearings without premagnetization.

[14] J. Hung 1995 *IEEE Trans. on Industry Applications* 31-6, 1492-1497. Magnetic bearing control using fuzzy logic.

APPENDIX

Finite Element Model of Stall-Rig:

No. of Element	DO	DI	E	G	RHO	LEN
1	14 ×25.4	0	2.07e10	6.9e11	7.8	0.7×25.4
2	14 ×25.4	0	2.07e10	6.9e11	7.8	0.7×25.4
3	5.25 ×25.4	3×25.4	2.07e10	6.9e11	7.8	1.25×25.4
4	3.75×25.4	1×25.4	2.07e10	6.9e11	7.8	1.0×25.4
5	3.75×25.4	1×25.4	2.07e10	6.9e11	7.8	1.25×25.4
6	3.75×25.4	1×25.4	2.07e10	6.9e11	7.8	0.5×25.4
7	4.25×25.4	1×25.4	2.07e10	6.9e11	7.8	5/8×25.4
8	8.25 ×25.4	4.8×25.4	2.07e10	6.9e11	7.8	2.5×25.4
9	8.25 ×25.4	4.8×25.4	2.07e10	6.9e11	7.8	3.0×25.4
10	8.25 ×25.4	4.8×25.4	2.07e10	6.9e11	7.8	0.5×25.4
11	6.20 ×25.4	4.8×25.4	2.07e10	6.9e11	7.8	3.0×25.4
12	6.20×25.4	4.8×25.4	2.07e10	6.9e11	7.8	3.0×25.4
13	6.20×25.4	4.8×25.4	2.07e10	6.9e11	7.8	3.0×25.4
14	6.20×25.4	4.8×25.4	2.07e10	6.9e11	7.8	2.75×25.4
15	6.20×25.4	0	2.07e10	6.9e11	7.8	5/8×25.4
16	3.30×25.4	0	2.07e10	6.9e11	7.8	1.75×25.4
17	3.30 ×25.4	0	2.07e10	6.9e11	7.8	1.5×25.4
18	3.30×25.4	0	2.07e10	6.9e11	7.8	1.75×25.4
19	7.30×25.4	0	2.07e10	6.9e11	7.8	5/8×25.4
20	7.30×25.4	0	2.07e10	6.9e11	7.8	5/8×25.4
21	3.50×25.4	0	2.07e10	6.9e11	7.8	1.25×25.4
22	3.50×25.4	0	2.07e10	6.9e11	7.8	0.75×25.4
23	8.25 ×25.4	0	2.07e10	6.9e11	7.8	1.25×25.4

where DO outer diameter, mm

DI inner diameter, mm

E Young's modulus, N/m^2

G elastic shear modulus, N/m^2

RHO mass density, kg/cm^3

LEN length of element, mm

Total number of elements: 23

Total number of nodes: 24